# Ensurance and simulation of electromagnetic compatibility: recent results in TUSUR University

Talgat Gazizov, Alexander Melkozerov, Alexander Zabolotsky, Sergey Kuksenko, Pavel Orlov, Vasiliy Salov, Roman Akhunov, Ilya Kalimulin, Roman Surovtsev, Maxim Komnatnov, Alexander Gazizov

***Abstract*—The paper presents and summarizes theoretical and practical results of recent electromagnetic compatibility (EMC) projects which are focused on the development of approaches, technologies and software for EMC of electronic equipment. Some representative results of EMC simulation and ensurance are presented. Outlook for applications of the obtained results in future projects of TUSUR University is given.**

***Index Terms*—EM software, EMC, signal integrity, simulation**

## I. Introduction

In the design of critical equipment it is necessary to take into account the requirements of the electromagnetic compatibility (EMC). These requirements continuously increase as the packaging density and upper frequencies of desired and noise signals in critical electronics grow. Actual EMC testing of the electronics and repetitive redesign due to failure to comply with increasingly strict EMC requirements considerably raise the price and duration of the design process.

A representative example of the critical equipment is a space vehicle. The EMC problem is especially of current concern for prospective space vehicles. Their distinctive features such as unified electronic modules based on the "system-on-a-chip" technology, unpressurised chassis and increased lifetime (up to 15 years and more) make the EMC ensurance and simulation even more difficult. In particular, increasing packaging density and, consequently, crosstalk in printed traces requires a signal integrity analysis. Unpressurised chassis worsens the shielding efficiency of the whole space vehicle for certain frequency ranges and requires special approaches to the simulation of chassis elements' shielding. Increased to 15 years lifetime makes the provision of significantly overestimated interference immunity margin necessary since noise electromagnetic excitations may grow during this period to such high levels which can be hardly predicted.

Therefore, careful analysis of a wide range of signal integrity, power integrity and EMC issues must be performed. However, focus on the analysis problems without computer-aided synthesis and optimization often makes the design ineffective and leaves hidden the resources for its improvement. To investigate these problems and develop appropriate solutions, a number of EMC projects was and being conducted at Tomsk State University of Control Systems and Radioelectronics (TUSUR University) for 2009–2016 years. Brief summary of new results on EMC simulation for space projects of TUSUR University, showing state of the art in the field to interested receachers has been presented recently [1]. The aim of this review paper is to present and summarize the results of the last projects and provide an outlook for applications of the obtained results in current projects. This paper is considerably extended: by representative data for the results only shortly described previously; by results not of simulation only but its application to ensure the EMC; by new results obtained not only in the space but other EMC projects.

Review of theoretical results were supported by RFBR grant 14-29-0925, practical results were supported by the state contract 8.1802.2014/K of the Russian Ministry of Education and Science, algorithms for accelerated linear systems solution were developed under RFBR grant 14-07-31267, analytical review of modal technologies is carried out at the expense of RSF grant 14-19-01232 in TUSUR.

All authors are with Department of Television and Control of Tomsk State University of Control Systems and Radioelectronics, Tomsk, Russia.

## II. Theoretical Results

### A. Quasi-static and Electromagnetic Analysis

Several derived analytic models [2] for time-domain response calculation of cascaded transmission line sections with capacitive loads have been implemented in the TALGAT software. Moreover, 4 new models for 2D configurations [3] and 2 new models for 3D ones [4] have been implemented for the analytical calculation of linear system matrix entries when obtaining the capacitive matrix of arbitrary structures. The program implementation allows computing the **L**, **C**, and **G** matrices for arbitrary interconnections of high complexity and density which are characteristic for the components of the "system-on-a-chip" type.

Simple, but representative example of the new 2D models usage is shown here on characteristic impedance ($Z$) estimations for three cases of a differential pair (Fig. 1). For ordinary case of rectangular conductors (Fig. 1(a)) $Z$=50.42 Ω. For the more real case of the curvilinear upper corners (Fig. 1(b)) $Z$=51.42 Ω that is by 2% more. At last, for previous case covered by CARAPACE EMP110 solder mask of thickness 20 μm and polyparaxylylene water resistant layer of thickness 15 μm, as taken from real world printed circuit board (PCB) of spacecraft, (Fig. 1(c)) $Z$=48.53 Ω that is by 4% less than in the first case. Such deviations are considerable for signal integrity, but can be controlled using the new models.

At last, the classical algorithm [5] using RWG-functions for electromagnetic analysis of arbitrary structures consisting of conductive patches has been improved by means of the calculation of the integrals using analytic formulas [6]. Comparative results of the first entry of **Z** matrix computation by these formulas and Newtone–Kotes integration for a plate of width 0.5λ excited by plane wave are shown in Table I.

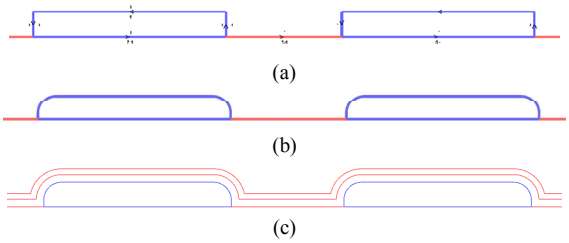


Fig. 1. Scaled cross sections of differential pairs of (a) rectangular, (b) curved, (c) curved and covered conductors

TABLE I.
THE RESULTS OF COMPUTING THE REAL AND IMAGINARY PARTS OF $Z11$

| Computing the integrals | Re($Z_{11}$), Ω | Im($Z_{11}$), Ω | $t$, ms |
|---|---|---|---|
| Numerical, accuracy 1 | $4.814\cdot10^{-8}$ | $-5.327\cdot10^{-9}$ | 95 |
| Numerical, accuracy 0.1 | $4.902\cdot10^{-8}$ | $-5.326\cdot10^{-9}$ | 453 |
| Numerical, accuracy 0.01 | $5.101\cdot10^{-8}$ | $-5.324\cdot10^{-9}$ | 1322 |
| Numerical, accuracy 0.001 | $5.293\cdot10^{-8}$ | $-5.327\cdot10^{-9}$ | 6000 |
| Analytic | $5.328\cdot10^{-8}$ | $-5.327\cdot10^{-9}$ | 502 |

From Table I one can observe that when increasing the integration accuracy the results obtained converge to those obtained by analytic formulas. However, the time of numerical integration increases (12 times for the integration accuracy equal to 0.001), whereas the time of computing the integrals by analytic formulas remains constant.

### B. *Solution of Linear Algebraic Systems*

The modeling in the range of parameters is often required. Example of the quasi-static problems is the capacitance matrix **C** calculation by method of moments for the frequency dependent dielectric constant. In this case, for each frequency a linear algebraic system is solved (order of the matrix $N$ is defined by a sum of subintervals on conductor $N_C$ and dielectric $N_D$ boundaries) with $N_{COND}$ (number of conductors in the structure) right hand side vectors. Thus, the time of calculation is proportional to the number of frequency points. However, for this case (of the dielectric constant variation), only the elements in the lower part of the main diagonal of the matrix (corresponding to the dielectric subintervals) are filled again for each frequency point. Therefore, the exploiting the incomplete change of the linear system matrix will significantly reduce the time of multiple calculations.

For this aim the block LU-decomposition is useful, wherein the original matrix is divided into blocks: $\mathbf{S}_{11}$ of size $N_C\times N_C$, $\mathbf{S}_{12}$ – $N_C\times N_D$, $\mathbf{S}_{21}$ – $N_D\times N_C$, $\mathbf{S}_{22}$ – $N_D\times N_D$. Only $\mathbf{S}_{22}$ entries are recalculated for each frequency point. The algorithm of the block LU-decomposition:

1. Assign $\mathbf{U}_{11} = \mathbf{S}_{11}$, $\mathbf{U}_{12} = \mathbf{S}_{12}$.
2. Calculate $\mathbf{L}_{21} = \mathbf{S}_{21}\mathbf{U}_{11}^{-1}$.
3. Calculate $\mathbf{U}_{22} = \mathbf{S}_{22} - \mathbf{L}_{21}\mathbf{U}_{12}$.

Obviously, the changing only the $\mathbf{S}_{22}$ diagonal entries changes $\mathbf{U}_{22}$ entries, because of (assigning $\mathbf{U}_{11} = \mathbf{S}_{11}^{-1}$ at the first step) all the remaining blocks ($\mathbf{U}_{11}$, $\mathbf{U}_{12}$, $\mathbf{L}_{21}$), including product $\mathbf{L}_{21}\mathbf{U}_{12}$, remain unchanged. Thus, for the $M$ calculations the only time consuming expansion of linear system matrix and subsequent $M$–1 computations of $\mathbf{U}_{22}$ block are needed. Obtained expression for the maximum acceleration for the block LU-decomposition at $M \to \infty$:

$$\beta = \lim_{M\to\infty} \frac{M\cdot T_{LU}}{T_1 + (M-1)\cdot T_S} = \lim_{M\to\infty} \frac{M\cdot T_{LU}}{T_1 + M\cdot T_S - T_S} = \frac{T_{LU}}{T_S},$$

where $T_1$ – time of the first solution, which includes inverting the $\mathbf{U}_{11}$ of size $N_C\times N_C$ and the subsequent solution of the linear system with finding right hand side vector; $T_S$ – time of computing the $\mathbf{U}_{22}=\mathbf{S}_{22}-\mathbf{L}_{21}\mathbf{U}_{12}$ and further solving the linear system. It is evident from the expression that the more the $M$, the smaller the acceleration depends on the time of the first solution. Moreover, the acceleration to a large extent depends on the size of the $\mathbf{S}_{22}$ block. Thus, for large $M$, $N$ and small $N_D$ the maximum acceleration of the multiple calculations can be obtained, whereas for small $M$ and large $N_D$ the acceleration will be negligible or not at all. The block LU-decomposition has been implemented and investigated for acceleration of multiple solution of linear equations with partly changing matrix. Acceleration by factor of more than 2 has been obtained for the simulation of the SNP 339 type connector. For particular structures, the acceleration can be up to factor of 35.

Obviously, if the analysis is required when changing the geometrical parameters of the structure, the matrix entries will vary in arbitrary places, and therefore the above-mentioned approach is not applicable. To overcome this problem a use of iterative methods was proposed.

The algorithm for multiple iterative solution of the linear system with partially changing matrix was presented in [7]. In this algorithm, the preconditioner matrix M is formed from the first linear system. Further, this matrix (without recalculation) is used for solving the following linear systems, thereby reducing the total solution time with acceptable accuracy. Finally, it was supposed that a similar algorithm can be applied when changing the sizes of the structure being analyzed. As a first step in this direction the reduction of the residual norm was investigated for solving the 10 linear systems, obtained by small changes for several parameters of a structure [8]. Example of these calculations for dielectric height ($h$) of microstrip line (Fig. 2) is presented in Fig. 3.

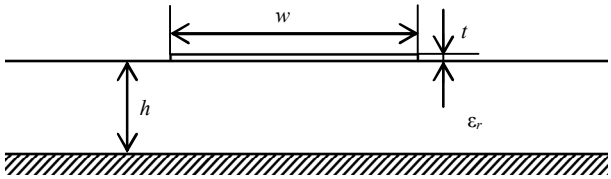


Fig. 2. Cross section of structure under consideration

All obtained results show that it is possible to use as a preconditioner the factorized matrix computed from initial parameters for multiple iterative solution of linear systems when changing the any parameters. But as the difference between the values of these parameters increases (by factor 2) the number of iterations also increases. Therefore, it is important to know the maximum number of iterations when the time required for solving by the iterative method is less than by the direct method. If the solution does not converged, then it is possible to recalculate preconditioner to get the solution convergence for total range of changing the parameters. In any case, the proposed approach may decrease considerably the time of multiple iterative solution of linear systems. Estimates of the speed up may be easily performed.

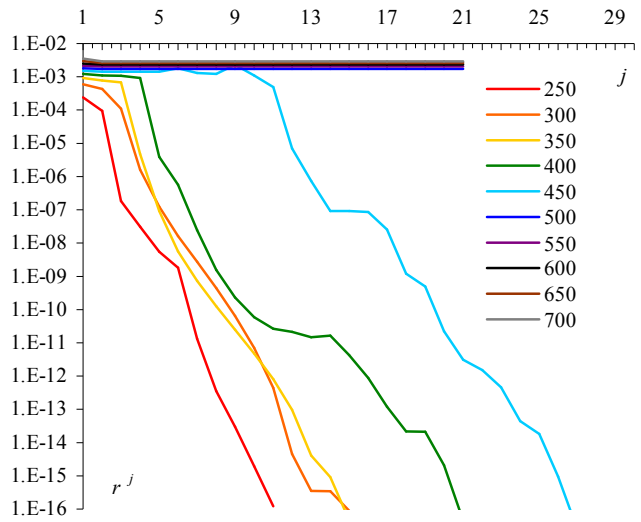


Fig. 3. Dependence of relative residual norm ($r^j$) on the number of iterations ($j$) for $h$=250, 300, ..., 700 μm

It was shown that the use of compressed sparse row format (CSR) for storing a preconditioner matrix is effective to reduce the computational cost. Acceleration of iterative solution of linear systems with dense matrices using sparse matrix storage formats has been considered in details [9]. Formulas for comparing the sparse matrix storage formats have been derived. An iterative algorithm for solving linear algebraic systems using sparse row format for storing prefiltered preconditioners has been designed. A modification of the sparse row format leading to 1.14–1.23-times speed-up for matrices of order 1000 has been suggested. It has been demonstrated that as opposed to the usual storage format, the sparse row format provides for 1.5–1.6-times speed-up in solving the linear systems of orders 4800, 6000, and 8000. The use of the obtained results allows one to reduce both memory and time requirements in solving large-scale problems with dense matrices.

Then, improvements to the ILU(0) factorization algorithm for preconditioning linear algebraic systems with dense matrices have been suggested [10]. (The preconditioner is stored in compressed sparse row format.) On the example of the problem of computing the electrical capacity of two stripes, it has been demonstrated that the modifications proposed provide for a significant reduction of the time for computing the ILU(0) preconditioner (up to 4 times) and for solving the preconditioned linear system (up to 2.5 times).

On real PCB structure problems, a new investigation has been performed in order to reveal the optimal value of the main parameter (drop tolerance) of the iterative solution of linear systems. The algorithm for calculation of capacitance matrices of structures of conductors and dielectrics using the method of moments has been improved for case of multiple calculations. The improved algorithm has been shown to work up to 4 times faster than the initial one.

The possibility of multiple iterative solution of linear systems was further investigated for computing the capacity of microstrip line in the wide ranges of its sizes.

To accelerate the iterative process two ways were considered. The first one is a use of a previous linear system solution (vector $\mathbf{x}_{i-1}$) as an initial guess for a following solution (vector $\mathbf{x}^0_i$), i.e. $\mathbf{x}^0_i=\mathbf{x}_{i-1}$ (for the first system a unit vector are used). The second one is the use of preconditioning matrix M, obtained by solving the first linear algebraic equation, i.e. $\mathbf{M}_i=\mathbf{M}_0$. In computational experiments four options were used: in option 1 acceleration was not used. In options 2 and 3, these ways were used separately, and in option 4 these ways were used together.

The previous structure (Fig. 2) was investigated. The aim of the experiment was to evaluate the time expenses required for the calculation of 100 capacitive matrices obtained by changing one of the dimensions of the structure: dielectric height $h$ (in the range of 12–112 μm or 933%); conductor width $w$ (in the range 18–118 μm, or 656%); conductor height $t$ (in the range of 6–106 μm, or 1767%). The number of segments on each boundary of structure has not changed, which allows for constant order $N$=1600 of the linear system matrices for correct comparison. As iterative method the BiCGStab method was chosen. Iterations were continued until the relative norm of the residual vector was more than $10^{-8}$. Gaussian elimination was used for comparison.

Ratios of the total (for 100 linear systems) solution times by Gauss elimination and by iterative method are shown in Table II for all options. Calculations have demonstrated the effectiveness of the proposed acceleration ways. The number of iterations when using the option 4 is minimal, that reduces the total time of 100 of linear systems solution by factor about 5–12 and proves the effectiveness of the combined usage of acceleration ways.

TABLE II.
TOTAL ACCELERATION OF MULTIPLE SOLUTIONS OF 100 LINEAR SYSTEMS FOR ALL OPTIONS

| Changed parameter | Option 1 | Option 2 | Option 3 | Option 4 |
|---|---|---|---|---|
| $h$ | 0.48 | 1.32 | 6.49 | 11.77 |
| $w$ | 0.31 | 1.15 | 5.87 | 10.98 |
| $t$ | 0.37 | 1.28 | 2.87 | 4.92 |

### C. *Modal Filtration*

Theoretical investigation of modal filtration in the printed circuit boards (PCBs), cables and separate modal block-filters led to the following results [11–13]. An important condition for the choice of the resistive loads at the ends of a modal filter (MF) section has been found which provides for equal magnitudes for the pulses decomposed at the filter output. An analytic expression for calculation of normalized magnitudes of the decomposed pulses as a function of wave impedance of even and odd modes has been derived. The dependency of these magnitudes on the coupling in the MF line has been demonstrated. Analysis of the power which is dissipated by resistors at the ends of active and passive conductors of multi-stage MF has been performed [14]. The analysis showed how one can select resistors by their dissipation power for given excitation parameters. A possibility to use widely available flat power cables as a protection against dangerous pulses by

means of decomposition into pulses with smaller magnitude has been revealed [15, 16]. This device has been shown to be radiation-resistant because it contains no semiconductor elements; cheap because besides the cable it contains just resistors; light and reliable since even short-circuits or gaps of cable conductors can be used instead of resistors. A modal block-filter structure with optimal parameters has been chosen. An experiment with a single-stage modal block-filter has been performed which validated the outcome of the theoretical investigation.

Cross section of the simplest (one-layer) planar structure comprising three conductors on one side of a dielectric substrate is shown in Fig. 4. Left conductor is active, central conductor is reference, and right conductor is passive.

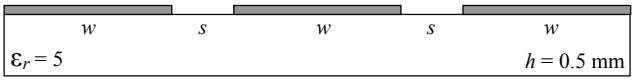


Fig. 4. Cross section of (one-layer) line section planar structure.

The typical length of printed coupled lines meandered on usual double-sided printed circuit board may be roughly assumed as 10 m for square of 1 dm$^2$. Therefore the difference of per unit of length delays of 1.3 ns/m (multiplied by the length) for these lines will allow decomposition of the pulses shorter than 13 ns. Use of two-layer structures is more preferable because the higher value of the difference of per unit of length delays permits to decompose longer pulses or, alternatively, to shorten the minimum length of a cable for previous pulse durations. For example, the improvement may be almost by factor of 1.5 in comparison with the one-layer structure. Use of high permittivity dielectrics allows improving the presented results proportionally to $\sqrt{\varepsilon_r}$, by factor of 6.

Cross sections of three conductor flat cables are shown in Fig. 5. All types of the cables have been classified in two kinds: with and without air gaps in cross section.

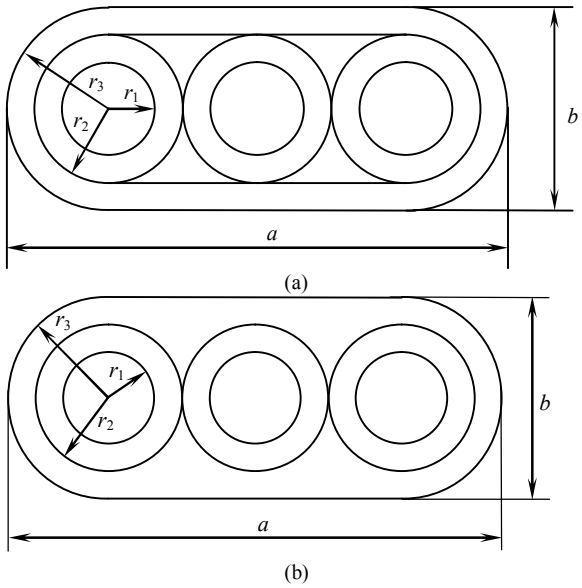


Fig. 5. Cross sections of cables with (*a*) and without (*b*) air gaps.

The typical length of low-voltage power cables may be assumed 10 m for domestic (room) and 100 m for floor (house) applications. Then the difference of per unit of length delays 0.3 ns/m (multiplied by the length) for these cables will allow dividing the pulses shorter than 3 ns and 30 ns accordingly. Use of cables without air gaps is more preferable because the bigger value of the difference 0.5 ns/m permits to extend the pulses up to 5 ns and 50 ns accordingly or, alternatively, to shorten the minimum length of a cable for previous pulse durations.

Modal filter consists of $N$ cascaded sections having the same cross sections but twice length (Fig. 6).

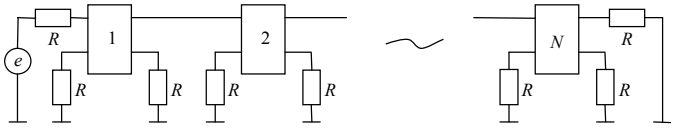


Fig. 6. Schematic of the modal filter.

To illustrate the functioning of the modal filter, we consider an example of the time-domain response calculation for excitation between signal (active) and reference conductors by short trapezoidal pulse. Rise, top and fall times for the pulse are equal to 100 ps each, while the magnitude on matched load is equal to 500 V. Waveform of the voltage between signal and reference conductors at the end of 6 cascaded sections is shown in Fig. 7. It is seen that an original pulse is decomposed to $2^6$=64 pulses. They must have magnitudes 500/64=7.8 V, but the observed magnitude is about 7.5 V, possibly, due to small mismatching. (It was assumed when modeling that losses and dispersion in lines are negligible.)

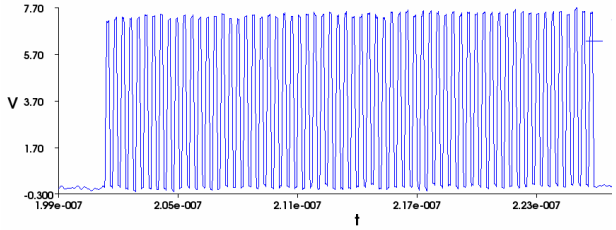


Fig. 7. Resulting waveform (V, s) of 500 V input pulse decomposition in printed modal filter into 64 pulses with small magnitudes (by factor of 64).

To obtain more proper $R$ value, an analytic expression for even/odd mode magnitudes (normalized to $E$ value) is used

$$U_{e,o}/E = (1+pL_{e,o})/2\cdot P_{e,o}, \quad (1)$$

where $pL_{e,o} = (R-Z_{e,o})/(R+Z_{e,o})$, $P_{e,o} = 1+R/Z_{e,o}$.

Equalization of even/odd mode magnitudes after simple manipulations gives the well known condition

$$R=(Z_eZ_o)^{1/2}. \quad (2)$$

Pulse magnitude for $R=(Z_eZ_o)^{1/2}$ is easy to obtain analytically, substituting (2) into (1), after simple manipulations as

$$U/E=(Z_e/Z_o)^{1/2}/((Z_e/Z_o)^{1/2}+1)^2. \quad (3)$$

This simple, but general formula expresses essentially the dependence of the one-stage MF attenuation on the coupling through the relation of even and odd mode impedances. Use of analytic formula (3) permits quick and accurate estimation of MF attenuation without computation of time domain response.

On condition (2) the voltage at the input of the filter is $U_0=E/2$. Then, assigning the output voltage of a stage by $U_1$, we have one-stage attenuation

$U_1/U_0=2(Z_e/Z_o)^{1/2}/((Z_e/Z_o)^{1/2}+1)^2$, (4)

and assigning $k=(Z_e/Z_o)^{1/2}$, we have simpler forms for 1 stage

$U_1/U_0=2k/(k+1)^2$ (5)

and $n$ stages

$U_n/U_0=[2k/(k+1)^2]^n$. (6)

The dependency of the power dissipation on the resistors of the $n$-stage MF on the input pulse duration $t_{in}=t_d+0{,}5t_r+0{,}5t_f$ (at the level of 0.5 of the magnitude) has been investigated and the following results have been obtained:

1. The power at the beginning of the passive conductor is distributed among the stages in proportion to their length.

2. The sum of average powers at the beginning of the passive conductor of all stages remains almost constant for MF implementations with any number of stages provided that the total mode delay difference is the same in all MF implementations.

3. The more stages are implemented in the MF, the bigger total power dissipates on the loads at the end of the passive conductor of all stages. This trend can be observed for all ranges under study (in the range as well as out of the range of MF effective filtration).

4. Increase in the number of the MF stages leads to the decrease of the MF effective filtration range since the input pulse energy distributes between the active and passive conductors equally.

5. If the stage length grows from the beginning to the end of the MF, the power which is dissipated on the resistors at the beginning of stages grows by factor of 2 from stage to stage; the power which is dissipated on the resistors at the end of stages decreases by factor of 2 from stage to stage.

## III. Practical Results

### A. Improved Simulation

The implementation of the improved iterative methods for solution of linear systems decreased the time needed for the EMC simulation of spaceborne equipment. The investigation of the spline approximation and the Godunov's method lead to the development of a universal instrument for approximation of different dependencies and alternative approach to the calculation of transmission line (nonregular and with non-linear loads) time-domain response. The usage of the alternative approach is useful for verification of the simulation results obtained by means of the main approach.

The application of the Godunov's method to such structures has been done for the first time. Numerical method of inverse Laplace transformation has been implemented as well. Response calculation results for structures of 1, 2, 3 line sections with linear and non-linear loads have been presented. To demonstrate the usage of the implemented methods, examples of the analysis of real electric interconnections in spaceborne equipment PCBs have been obtained.

Capacitances for different real 3D-structures of spaceborne equipment have been calculated: contact pads, footprints, crossing of two conductors, interlayer via, SNP 339 connector.

Analytic models for shielding effectiveness (SE) calculation of typical structures (metal plate and rectangular chassis with a slot) suitable for quick estimations of real spaceborne equipment structures have been implemented. These models have been tested on the following comparative estimations: magnesium alloy and aluminum plates, UEM case of various sizes, connector case with an overlapping slot. Example of electric field SE frequency dependence calculated for a distance of 1 mm from the metal plate is shown in Fig. 8(a). One can see a presence of the pronounced SE minimum, because of which the SE is reduced at some frequency range with increasing the frequency. For copper, the minimum corresponds to the frequency of 0.1 MHz, for aluminum – 0.2 MHz, and for magnesium alloy – 1 MHz. It is the presence of this minimum that leads to the existence of the frequency range on which the SE degradation increases with increasing the frequency. For example, the SE at the frequency of 0.2 MHz is reduced by 20 dB, whereas at 1 MHz – 30 dB. It is worthy of note that this minimum dropouts with the plate thickness increasing, as shown in Fig. 8(b). Therefore, similar estimations are relevant also for a thin foil.

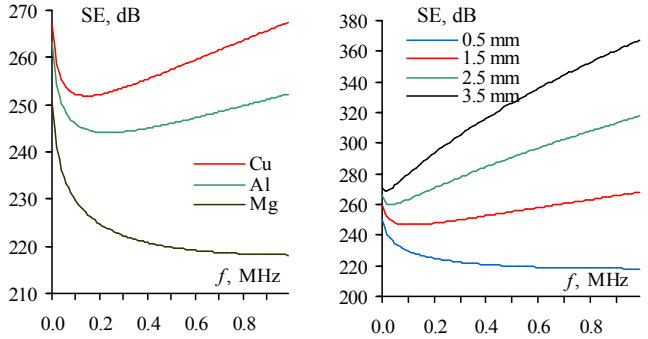


(a) (b)

Fig. 8. Frequency dependence of electric field SE at a distance 1 mm from a plate: (a) of thickness 0.5 mm for different metals; (b) of thickness 0.5–3.5 mm for magnesium alloy

Example of SE connector case (Fig. 9) estimation, being actual for protection of sensitive circuits' junctions for a spacecraft with unpressurised chassis from external fields, is shown in Fig 10. It shows the influence of the aperture ($w$) of the front wall of the connector case ($a\times b\times d$=29.5×8×21.5 mm) in the frequency range up to 20 GHz. From Fig. 10 one can see that at frequencies up to 1 GHz for the gap aperture of 2 mm SE value increases about 20 dB in comparison with a fully open aperture, while in the intervals between the resonant frequencies it increases about 10 dB, whereas at the resonance frequencies the SE may degrade.

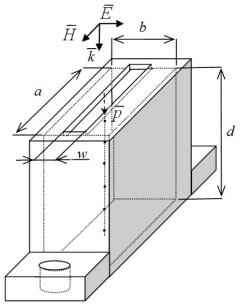


Fig. 9. A model of connector case

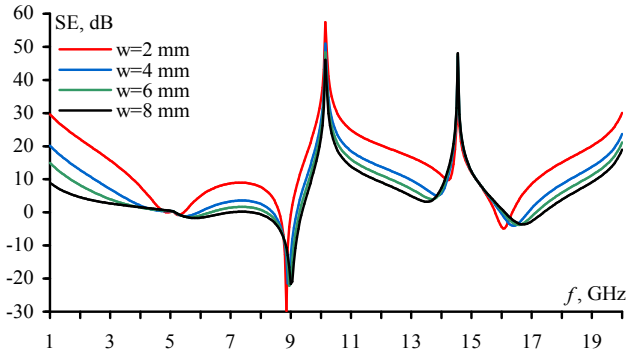


Fig. 10. Frequency dependence of SE inside of the connector case at distance $p$=10 mm

## B. Modal Technologies

A technology for reduction of signal distortion in the printed conductors using optimal choice of conductor and dielectric parameters has been proposed. To decrease modal distortion in active conductor and far-end crosstalk in structures with nonhomogenous (in cross-section) dielectric filling, an additional dielectric layer (such as moisture-protective coating layer) covering the PCB surface has been proposed. The applicability of this technology has been verified by simulation of a real PCB fragment. The value of this technology consists in its implementation without either change of routing or introduction of additional components. Only the optimal varnish thickness must be selected at the latest stage of the PCB manufacture. This can be easily done, for example, by means of the polyparaxylylene covering with precisely controlled thickness. The described technique is demonstrated by the simulation of the eight-wire bus of the spacecraft PCB (Fig. 11).

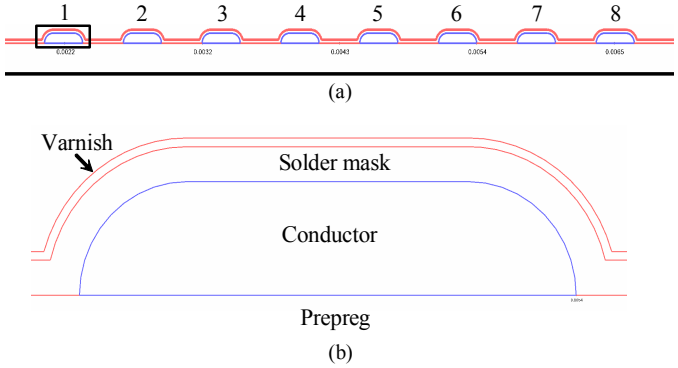


Fig. 11 Eight-wire bus: (a) cross section and (b) increased fragment of it

Thickness of a covering varnish $hV$ is changed with fixed other parameters. The near end of the outer conductor was excited by the trapezoidal pulse (EMF of 6 V, front/decay duration of 1 ns, flat top duration of 8 ns). The crosstalk waveforms at the ends of passive conductors of the bus are shown in Fig. 12 (for case of 5 Ω at the near ends and 1 MΩ at the far ends of passive conductors) for different $hV$ values. One can observe the original crosstalk level of 2 V for $hV$=5 μm and the crosstalk reduced down to 0.8 V for $hV$=100 μm.

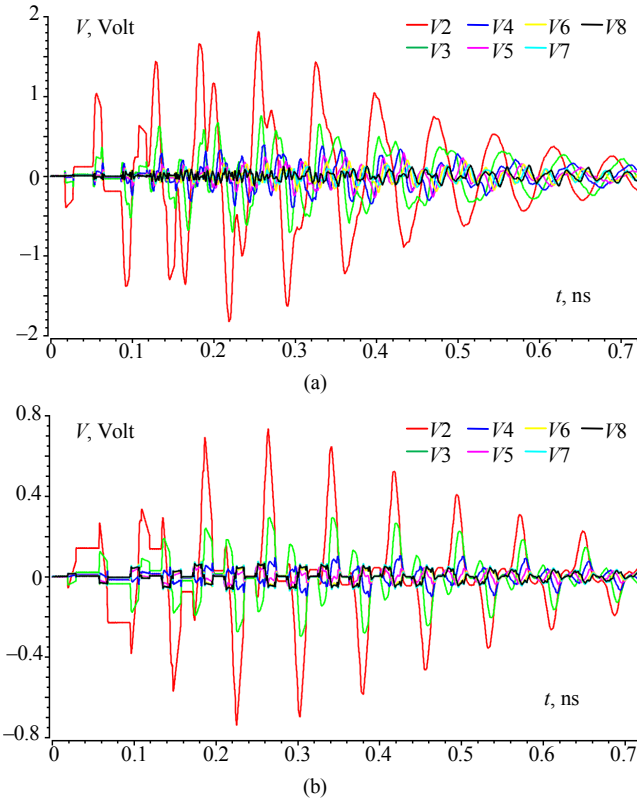


Fig. 12. Far-end crosstalk waveforms of eight-wire bus for varnish thickness of (a) 5 and (b) 100 μm

A modal filtration technology has been developed and patented [17] which is based on a new principle of protection against short pulses with dangerously high voltage in transmission lines. It uses the phenomenon of pulse signal decomposition in cascaded transmission line sections. Application of this technology allows improving the conducted susceptibility of power and signal circuits of PCBs with "system-on-a-chip" components. Analysis and implementation of modal filtration in various elements of spaceborne equipment yielded the following results: the manufacture of PCBs with integrated modal protection has been proposed; calculation of MF characteristics for nominal values of PCB fiber glass and foil thicknesses; MF calculation sequence has been presented; possible options for structural implementation of MF have been proposed; an experimental investigations of ultra-short pulse propagation in 6 prototypes of single-stage MF with the broad side coupling (as the most promising), frequency characteristics of 2 prototypes as well as ultra-short pulse propagation in MF based on the flat cable have been performed. A general technique for separate and joint (with traditional protection methods) usage of modal filters has been presented [18]. The application of the steps of the technique for creation of MF based on the flat printed cable or of the printed MF has been shown. Design documentation has been developed for printed MF production.

To illustrate this results a symmetrical structure of single-stage MF with the broad side coupling is shown in Fig. 13, where A, P, R denote active, passive, and reference conductors, accordingly, while $R$ is resistance value.

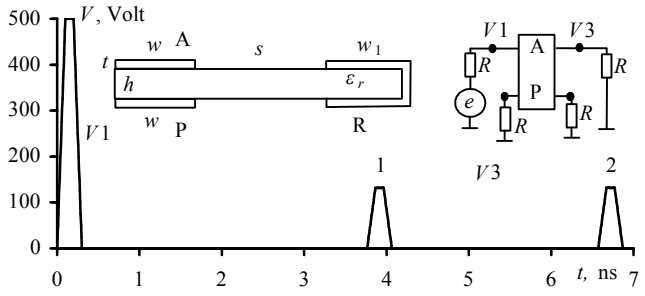


Fig. 13. Cross section of symmetrical modal filter structure, schematic of the connections and waveforms of the voltage at the active conductor

The following features of this structure are observed. The active and passive conductors and reference conductor as well are axially symmetric. Width of conductors ($w$, $w1$) may be increased for high current, while the separation of conductors ($s$) may be used in order to keep the defined value of characteristic impedance. However, the main advantage of this structure concludes in the fact that the odd mode propagates mainly in dielectric substrate, while the even mode propagates only partly in dielectric substrate, but considerably – in air.

Cross section of other (asymmetric) structure of MF is shown on Fig. 14. Peculiarity of this structure is the absence of the U-shaped strip line that simplifies MF placement on the PCB. As the result the excitation pulse magnitude is decreased by factor 5 for the difference of modal delays of 3 ns/m with MF length of 0.2 m.

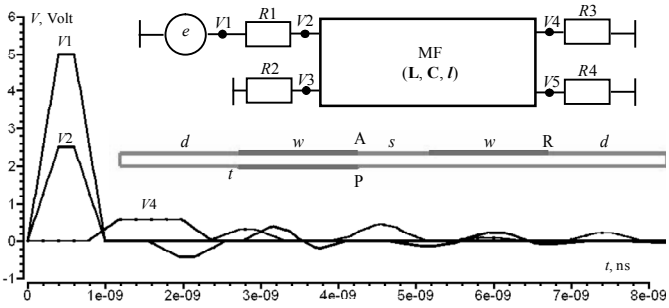


Fig. 14. Cross section of asymmetrical modal filter structure, schematic of the connections and waveforms of the voltage at the active conductor

A technology of modal decomposition and restoration, or "modal excitation" in short, has been proposed and patented [19] in order to reveal hidden possibilities of modal decomposition and restoration of pulse and harmonic excitations with dangerous magnitude in spaceborne equipment structures.

An essence of the modal decomposition and restoration phenomenon consists in the following. If the protective equipment (PE) is included between a signal and reference conductors before the protected circuit, the dangerous pulse may decompose into pulses with smaller magnitude at the end of section 1 (Fig. 15). As the result the PE will not protect if the amplitude of the decomposed pulses is below the threshold of the PE sensitivity. Moreover at the end of section 2 restoration of dangerous pulse can happen because the modes simultaneously come at the end of section 2. As the result it may destroy the functioning the subsequent circuits.

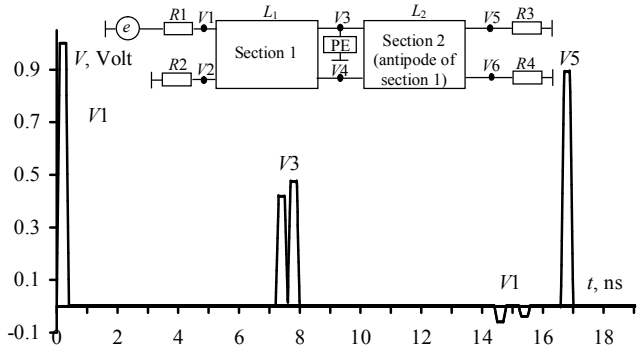


Fig.15. Schematic of the connections and waveforms of the voltage

The modal antipodes are the segments of coupled lines wherein the per unit of length propagation delays of odd and even modes are equal in magnitude but opposite in sign. Since the difference of the modal delays of coupled lines is determined by its length multiplied by difference of the per unit of length propagation modal delays it is last is determining the sign of the difference of the modal delays. Therefore, this is important to investigate in future the modal antipodes for various real structures.

The modal probing technology has been proposed for contactless detection, identification and diagnostics of multiconductor interconnects. Two implementation options (active [20] and passive [21]) have been patented. Under detection the ability to detect passive (probed) conductors is meant. Under the identification the ability to determine the amount of probed conductors is meant. Under diagnostics the ability to determine passive (probed) conductors breaking is meant. It is known that the pulse signal in the $N$-conductor (not including the reference) line with an inhomogeneous dielectric filling may be subjected to modal distortion up to modal decomposition on $N$ pulses of smaller amplitude due to differences of modal delays. Complete decomposition of pulse signal in the line with length $l$ will occur if the total pulse duration $t_\Sigma$ less than the minimum modulus of the difference mode delay propagation in structure, i.e. under the condition

$$t_\Sigma < l \cdot \min|\tau_i - \tau_k|, \quad i, k = 1, \ldots, N, \quad i \neq k,$$

where $\tau_{i(k)}$ – delay per unit of length for $i(k)$-th mode of structure. This phenomenon can be applied for detection, identification and diagnostics of multiconductor interconnects. Generalization of these opportunities herein is called the modal probing. If probed conductors have different electrical and magnetic couplings with the probing line, the information about probed conductors can be obtained from the form of modal signal distortion in the probing line.

Block diagram of the device that implements the principles of modal probing is shown in Fig. 16. The device operates as follows: the probing pulse from the generator output goes to a probing line. The probing pulse passing along the probing line is subjected to modal distortion caused by the presence of probed wire structure. The receiver gets the signals from the input and output of the probing line and sends information to the processing unit. All units of the device function according to signals of control unit. From the shape of the signals at the

near and far ends of the probing line information about the probed structure is obtained.

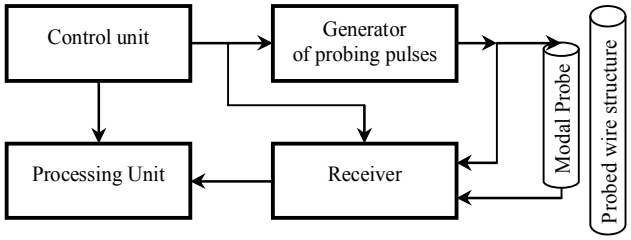


Fig. 16. Block diagram of the active modal probing device

The possibility of detection and identification of electrical interconnections by modal probing is illustrated by quasi-static modeling of the trapezoidal pulse (keystone-shaped) signal distortion in the microstrip structures 1.5 m in length (Fig. 17). For $N$=2 (Fig. 17*a*) at the far end of the probing line ($V3$) there are two pulses rather than one. The second pulse was caused by the presence of the probed passive wire (and, as a consequence, by the excitation of even and odd modes), electric and magnetic couplings with the probing line, and by the fact that the total duration of the input pulse was less than the total difference between modes delays. The difference of modes delays is due to the inhomogeneous dielectric filling of structure. For $N$=3 (Fig. 17(b)) at the far end of the probing line ($V3$) there are three pulses rather than two. The appearance of three pulses is caused by the presence of two passive conductors, so three modes are excited in the structure and the delay difference between them is more than the pulse duration.

Thus, these results show that using the number of pulses at the far end of the active conductor one can determine the presence and amount of passive conductors i.e. solve the problem of detection and identification of electrical interconnections.

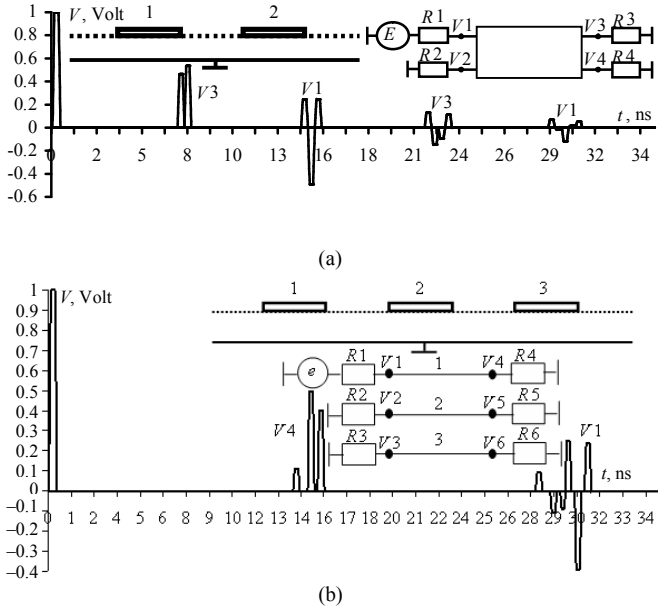


Fig. 17. The waveforms at the input and output of active microstrip line when (a) $N$=2 and (b) $N$=3

The possibility of diagnostics is illustrated by results of simulation and experiment of the pulse propagation along the flat cable of the PUGNP 3×1.5 type (Fig. 18*a*).

For the diagnostics of a passive wire by the modal probing the form of a modal distortion of the pulse signal should vary depending on the condition of passive wire. One of the important problems of electrical connections diagnostics is to determine the wire breaks. Let's consider in Fig. 18(b) an effect of passive wire break to a form of modal distortion of the pulse signal in the probing line. The waveform at the far end of the probing line is shown in Fig 19. As can be seen, when passive wire is break, four pulses come to the far end of the probing line instead of two as in the case without break. (Partial overlap of the pulses is due to dispersion.) Waveforms at the far end of the probing line under various boundary conditions at the ends of the passive wire are considered in more detail in [22]. Modal distortion in frequency domain is considered in [23].

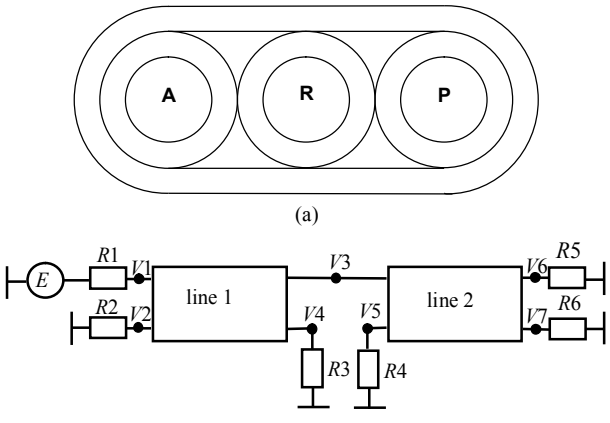


Fig. 18. Cross section (a) of the 3×1.5 flat cable of the PUGNP type and (b) schematic diagram of the examined structure with break in passive wire

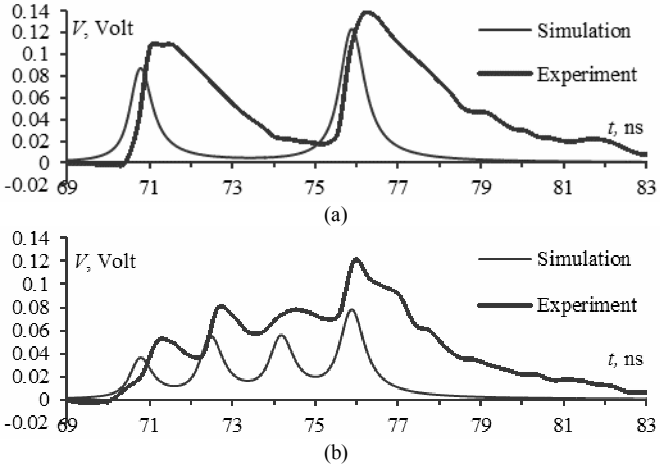


Fig. 19. The waveforms at the far end of flat cable (a) without and (b) with passive wire break

### *C. Environmental shielded TEM chamber*

At the present time the measurement systems for EMC testing, based on various methods and equipment are actively improving. One way to improve the characteristics and to enhance the tests conducted using various equipment is their hybridization. For this propose the idea of integration of TEM-

cell into the environmental shielded chamber is proposed and actively developed. It will permit to gain new knowledge about the interaction between internal and external electromagnetic and climatic effects on a TEM-cell and a device under test (DUT), located in the internal volume of the TEM-cell. Besides, it will help to bring the EMC tests (measurements of emission and immunity) to the real operating conditions of the DUT. For practical purposes, it will be possible, for example, to identify failure mechanisms in semiconductor components subjected to the thermal and electromagnetic fields. This is important when the component is operating at limits of the temperature range where the risk of failure of its p-n junction due to the cumulative effects of various factors (including an ultra wide band pulse) raises. The above-described concept is implemented in a new type of chamber (Fig. 20).

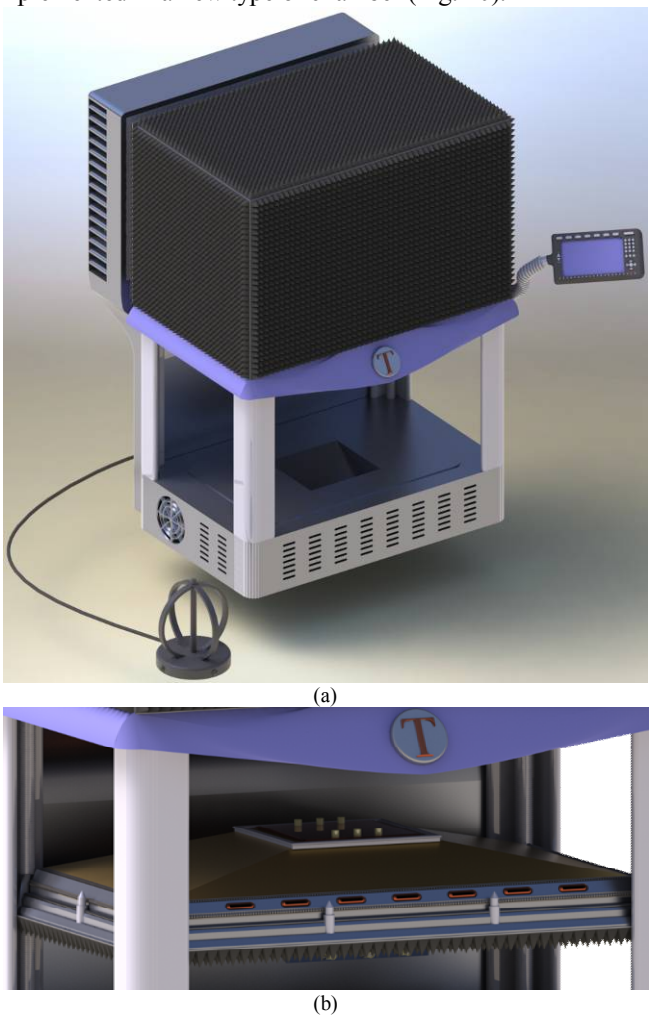

(a)

(b)

Fig. 20. Environmental shielded TEM chamber: (*a*) exterior, (b) view with the open door

The chamber design shown in Fig. 20(a) includes an outside case with multilayer shield and RF absorber; external sensor of temperature and electromagnetic field; MPU control system; LCD display for digital and graphic visualization of the temperature and humidity inside the TEM-cell, automated removable door at the bottom shown in Fig. 20(b), on the inner side of which a test table is placed for the DUT, occurring inside the TEM-cell after closing (lifting up) the door. The chamber will allow for research and EMC testing of a component or a small device on single and joint effects of temperature and humidity, as well as measurements of emissions from it.

Also, with this chamber one can get more advanced Spice, IBIS and ICEM models of components. Particularly, research and testing of new components (modal filters) family is planned in this chamber.

The methods of component tests are based on EMC standards, in particular on emission and immunity tests of IC, and also include common standards for EMC testing of radioelectronic equipment in TEM-cells. During these tests the DUT characteristics are measured in wide frequency range (up to 3 GHz) when exposing to electric field (up to 3 kV/m) with temperature (–50 to +150°C) and humidity (up to 90%). SE of the chamber case is more than 40 dB at frequencies up to 40 GHz.

### *D. Other Results*

The optimization of spaceborne equipment by EMC criteria (EMC optimization in short) is characterized by a large number of parameters and local optima of the objective function in conjunction with resource-intensiveness and diversity of the underlying analysis problems. Even the application of evolutionary algorithms which is the most appropriate option for such optimization problems becomes increasingly complicated as the complexity of the prospective space vehicle EMC simulation grows. Therefore, it is necessary to enhance the existing optimization algorithms and propose techniques for their effective usage in practice. To this end, a technique for EMC optimization of spaceborne equipment has been developed and its main steps have been described. The technique has been tested on several examples of parameter optimization: a microstrip line, a wide-band mathematical model of resistor including parasitics, a multiconductor transmission line as well as structural optimization of multi-stage MF.

Preliminary simulation of EMC testing in accordance with MIL-STD-461F standard has been implemented in the part of conducted emissions from power circuits of the “system-on-a-chip” components.

Preliminary measurement results of the reflection ratio $S_{11}$ in the frequency range from 10 MHz to 20 GHz have been presented for two typical components (capacitor and resistor). A significant difference between characteristics of idealized elements, classical model and real components has been demonstrated.

Below the creating the models of the SMD resistor and the wired capacitor is briefly described. For this aim the following technique was used: 1) measurement of reflection coefficient $S_{11}$ frequency dependence for a component; 2) calculation of impedance $Z$ from $S_{11}$; 3) approximation of the $Z$ frequency dependence by a rational function; 4) expansion of the rational function on partial fractions; 5) realization of partial fractions by the equivalent circuits, using the methods of circuit synthesis; 6) generation of total SPICE-model; 7) model verification.

Measurement of $S_{11}$ is performed on the vector network analyzer. For performing the measurements the components are soldered on SMA connector of coaxial-microstrip transition type [24]. To reduce the transition influence the connector pin was previously shortened.

After calculation of $Z$ from $S_{11}$ the approximation of $Z$ by a rational function using the vector fitting method [25] is performed. As a result the following rational function is obtained

$$f(s) = \sum_{m=1}^{N} \frac{c_m}{s - a_m} + d + se \cdot \tag{7}$$

The first member of the function is decomposed into several sums of fractions with complex conjugate poles of the form

$$\frac{a + jb}{s - (\sigma + j\omega)} + \frac{a - jb}{s - (\sigma - j\omega)}. \tag{8}$$

Each such sum (8) is realized as a parallel *_pi* circuit (Fig. 21), but the remaining members – as cascaded resistance and inductance. To calculate the parameters of the circuit for the resistance and inductance the formula from [26] are used. Total equivalent circuit for the resistor is consisting of 4 cascaded parallel circuits, resistance and inductance and for the capacitor – of 6 circuits.

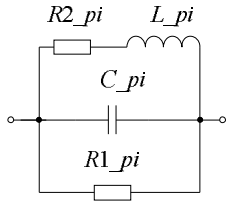


Fig. 21. Schematic of the parallel circuit

For verification of the models their circuit analysis in TALGAT system was made. The frequency dependences of $Z$, calculated using the obtained models of the resistor and capacitor are shown in Fig. 22.

Root mean square deviations (RMS) between results of $|Z|$ measurement and modeling are equal to 0.701 Ω for the resistor, and 11.05 Ω for the capacitor. Thus, it is possible to conclude that the obtained models are exact and suitable for PCB EMC analysis.

To import real PCB configurations and prepare them for EMC simulation, a TLPCB conversion module has been created. Commands implemented in the TLPCB module allow reading the PCB designed in Altium Designer into the memory and convert it into a format suitable for further processing using the TALGAT software. Example of these automatic transformations is demonstrated in Fig. 23, wherein firstly a net *A*-*B* is chosen with defined distance (*s*) to account for presence of neighboring conductors and cross sections of the resulting structure are obtained consequently at distance of *d*, then 6 intervals (*len*1–*len*6) having the unique sections are revealed using a graph theory, at last, circuit diagram consisting of cascaded multiconductor transmission lines described by according **L**, **C**, **R**, **G** matrixes is obtained. One can observe that mutual couplings of neighboring conductors can be properly and automatically considered.

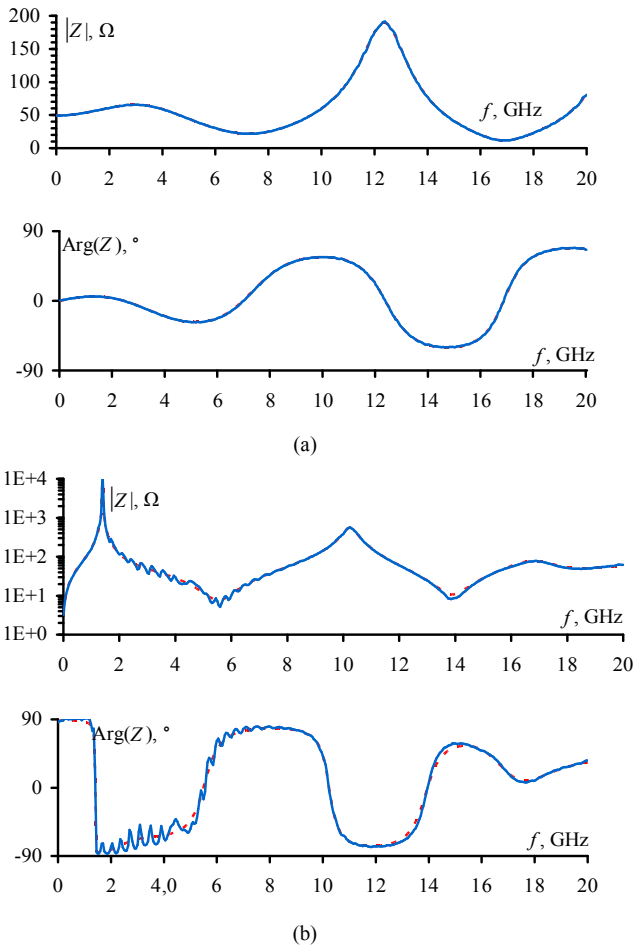


Fig. 22. Frequency dependence of impedance $Z$ for (a) resistor and (b) capacitor: measurement (–), modeling (– –)

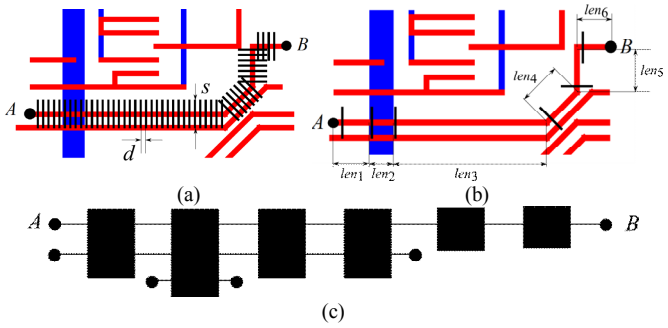


Fig. 23. Automatic transformations of (a) printed nets to (b) line intervals and (c) to a circuit diagram

As a further extension of this PCB import the capability of more detailed representation of the wide bus bending is implemented for more precise simulation of high speed signals propagation. It is schematically shown in fig. 24.

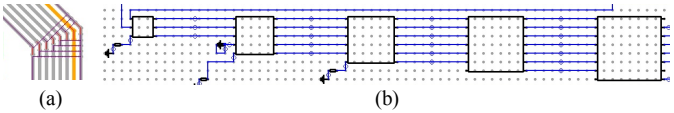


Fig. 24. Sketch of (a) bus bending and of (b) a halve of its precise circuit presentation

A technique for preliminary EMC analysis of PCBs based on qualitative analysis (without simulation) has been developed

which allows for obtaining of specific recommendations for improvement of the EMC of PCBs without knowing details of PCB circuitry engineering and just by changing the PCB routing. The technique has been tested by preparation of preliminary recommendations for 5 real PCB. All recommendations have been taken into account by designers, and according to a number of recommendations (about 100), changes in the PCB routing have been introduced. Similarly, recommendations for a more complex PCB (radio navigation electronic equipment unit of spacecraft) have been developed.

Techniques for obtaining of Spice-models have been developed for the following analog components: capacitor, resistor, diode, bipolar transistor. Technique for creation of models has been developed which takes into account parasitic parameters. For some integrated circuits (IC) and analog components the preliminary models have been created. Techniques for creation of IBIS-models based either on physical measurements or Spice-model conversion have been developed. An example of database for ICs used for spaceborne equipment has been created.

The results of the improvement of the technique for preliminary EMC analysis of PCBs have been presented for routing of back-up circuits. The proposed approach for reduction of radiated emissions has been shown to be effective for the open structure as well as in the presence of conductive plate and shielding box.

The results of the usage of simulation for preparation of recommendation to ensure the EMC have been presented for PCB power-ground circuits. A possibility to decrease the inductance of power-ground circuits by factor of 9 by means of conductor routing has been shown.

The following programs and techniques have been developed for real PCBs: programs and technique for simulation of electric circuit which take into account parasitic parameters of components and PCB; a technique for search for circuit parts with problems; a technique for signal integrity analysis of real PCB in Altium Designer; a technique for post-topological analysis of crosstalk in Altium Designer; a technique for signal integrity analysis using TALGAT software; program and techniques for electromagnetic simulations.

## IV. Conclusions and Outlook

In the paper, the results of the recent EMC projects have been presented and summarized. First, the outcome in the field of quasi-static and electromagnetic analysis has been described, in particular, models for calculation of time-domain response and capacitive matrix. After that, improvements for solution of linear algebraic systems and corresponding speed-ups (up to 12 times) have been discussed. Then modal filtration in PCBs has been considered.

The practical significance of the obtained results has been highlighted in the second section where details about developed methods for improved EMC simulation have been provided, including the spline approximation, the Godunov's method, the analytic models for SE calculation of typical structures. Technologies for reduction of signal distortion, modal filtration, modal decomposition and restoration and modal sensing have been presented with corresponding references. Finally, proposed techniques for EMC improvement of spaceborne equipment have been briefly presented. A number of theoretical and practical results obtained are used and will be implemented in the new project on the development of prospective equipment for global navigation satellite system. The simulation of this equipment will be performed using the TALGAT software which includes models and features developed during the past project and modified during the new project. Application of the techniques presented in the paper will guarantee high functional and EMC characteristics of the prospective equipment. At last the obtained results have formed a base for their extensions in the current and future EMC projects of TUSUR University.

## References


[1] T. Gazizov, A. Melkozerov, A. Zabolotsky, P. Orlov, V. Salov, R. Ashirbakiev, R. Akhunov, S. Kuksenko, I. Kalimulin, "New results on EMC simulation for space projects of TUSUR University," Proc. of IEEE Int. Conf. on Numerical Electromagnetic Modeling and Optimization for RF, Microwave, and Terahertz Applications. May 14–16, 2014, Pavia, Italy.

[2] T.R. Gazizov and N.A. Leontiev, "Transient response of a periodic transmission line structure with capacitively loaded junctions," Proc. of the 1997 Sino-Japanese Joint Meeting on Optical Fiber Science and Electromagnetic Theory. October 14–16, 1997, Wuhan, China, pp. 322–327.

[3] T.R. Gazizov, "Analytic expressions for Mom calculation of capacitance matrix of two dimensional system of conductors and dielectrics having arbitrary oriented boundaries," Proc. of the 2001 IEEE EMC Symposium, Montreal, Canada, August 13–17, 2001, vol. 1, pp. 151–155.

[4] T.R. Gazizov, "Calculation of capacitance matrix of three dimensional multiconductor system in multiple dielectric media," Record of International Symposium on Electromagnetic Compatibility. Magdeburg, Germany, October 5–7, 1999, pp. 31–36.

[5] S.M. Rao, D.R. Wilton, A.W. Glisson, "Electromagnetic scattering by surfaces of arbitrary shape," IEEE Transactions on antennas and propagation, May 1982, vol. 30, no. 3, pp. 409–418.

[6] I.S. Kostarev, T.R. Gazizov, Yu.M. Kazantsev, "Analytic evaluation of the matrix entries for linear algebraic systems in the problem of electromagnetic scattering by surfaces of arbitrary shape," Journal of Mathematical Sciences, Vol. 199, no. 4, June, 2014, pp. 456–462.

[7] R.R. Akhunov, S.P. Kuksenko, V.K. Salov, T.R. Gazizov, "Multiple iterative solution of linear algebraic systems with a partially varying matrix," Journal of Mathematical Sciences, Vol. 199, no. 4, June, 2014, pp. 381–385.

[8] V.K. Salov, T.R. Gazizov, O.A. Nikitina, "Convergence of multiple iterative solution of linear algebraic systems with a fully varying matrix using a single calculated initial preconditioner," Innovative Information Technologies: Materials of the International scientific-practical conference. Part 2. / Ed. Uvaysov S.U.–M.: HSE, 2014. April 21–25, 2014, Prague, Czech – P. 452–457.

[9] R.R. Akhunov, S.P. Kuksenko, V.K. Salov, T.R. Gazizov, "Sparse matrix storage formats and acceleration of iterative solution of linear algebraic systems with dense matrices," Journal of Mathematical Sciences, vol. 191, May, 2013, pp. 19–27.

[10] R.R. Akhunov, S.P. Kuksenko, V.K. Salov, T.R. Gazizov, "Optimization of the ILU(0) factorization algorithm with the use of compressed sparse row format," Journal of Mathematical Sciences, vol. 191, May, 2013, pp. 19–27.

[11] T.R. Gazizov, A.M. Zabolotsky, I.E. Samotin, "Modal decomposition of UWB pulse in power cable structures: simple experiment showing useful possible applications," Book of abstracts EUROEM 2008, 21–25 July 2008, Lausanne, Switzerland, p. 62.

[12] T.R. Gazizov, I.E. Samotin, A.M. Zabolotsky, A.O. Melkozerov, "Design of printed modal filters for computer network protection," Proc.

of 30-th Int. conf. on lightning protection, Sept. 13–17, 2010, Cagliary, Italy, pp. 1246-1–1246-3.
[13] T.R. Gazizov, A.M. Zabolotsky, A.O. Melkozerov, E.S. Dolganov, P.E. Orlov, “Improved design of modal filter for electronics protection,” Proc. of 31-st Int. conf. on lightning protection, Sept. 2–7, 2012, Vienna, Austria, pp. 1–4.
[14] T.R. Gazizov, A.M. Zabolotsky, A.O. Melkozerov, E.S. Dolganov, P.E. Orlov, “Analysis of power dissipation in resistive terminations of single- and multistage modal filters,” Proc. of 31-st Int. conf. on lightning protection, Sept. 2–7, 2012, Vienna, Austria, pp. 1–4.
[15] T.R. Gazizov, A.M. Zabolotsky, “Experimental results on UWB pulse propagation in low-voltage power cables with different cross sections,” IEEE Transactions on electromagnetic compatibility, vol. 54, no. 1, February 2012, pp. 229–231.
[16] T.R. Gazizov, A.M. Zabolotsky, I.E. Samotin, A.O. Melkozerov, “Simple and free mitigation of short pulse lightning effects by flat power cables,” Proc. of 30-th Int. conf. on lightning protection, Sept. 13–17, 2010, Cagliary, Italy, pp. 993-1–993-3.
[17] Patent of Russian Federation №2431897.
[18] T.R. Gazizov, A.M. Zabolotsky, A.O. Melkozerov, P.E. Orlov, I.G. Bevzenko, E.S. Dolganov, “Evaluations of protection methods using TVS-array and modal filter,” Book of abstracts EUROEM 2012, 2–6 July 2012, Toulouse, France, p. 106.
[19] Patent of Russian Federation №2431912.
[20] Patent of Russian Federation №2386964.
[21] Patent of Russian Federation №2456588.
[22] P.E. Orlov, T.R. Gazizov, A.M. Zabolotsky. Experimental confirmation of the possibility for contactless diagnostics of multiconductor structures using modal probing // Russian Physics Journal. November 2013, Volume 56, Issue 6, pp 652–656.
[23] P.E. Orlov, T.R. Gazizov, A.M. Zabolotsky. Frequency Analysis of Modal Distortions and its Application to Diagnostics of Electric Connections // Russian Physics Journal. January 2014, Volume 56, Issue 9, pp 1099–1101.
[24] I.F. Kalimulin, T.R. Gazizov, A.M. Zabolotsky “Impedance of low-frequency passive components of spaceborne equipment at frequencies ranging to 20 GHz,” Instruments and Experimental Techniques, vol. 55, no. 2, pp. 231-237, 2012.
[25] B. Gustavsen, “Improving the pole relocating properties of vector fitting,” IEEE Trans. Power Deliv., vol. 21, no. 3, pp. 1587–1592, 2006.
[26] N. Balabanian, Network Synthesis. Englewood Cliffs: Prentice-Hall, 1958, p. 440.